Quadrupolar ordering and magnetic properties of tetragonal $TmAu_2$

Masashi Kosaka,* Hideya Onodera, Kenji Ohoyama, Masayoshi Ohashi,† and Yasuo Yamaguchi
Institute for Materials Research, Tohoku University, Katahira 2-1-1, Sendai 980-77, Japan

Shintaro Nakamura‡ and Terutaka Goto§
Research Institute for Scientific Measurements, Tohoku University, Katahira 2-1-1, Sendai 980-77, Japan

Hisao Kobayashi
Graduate School of Science, Tohoku University, Aramaki, Sendai 980-77, Japan

Susumu Ikeda
National Laboratory for High Energy Physics, Oho 1-1, Tsukuba 305, Japan
(Received 29 August 1997; revised manuscript received 22 May 1998)

Magnetic susceptibility, magnetization process, specific heat, ultrasonic velocity, and inelastic neutron scattering experiments were performed on powdered and single-crystalline $TmAu_2$ samples. $TmAu_2$ with a simple body-centered tetragonal $MoSi_2$-type structure undergoes a transition to an antiferromagnetic state at T_N of 3.2 K. An anomaly at 7.0 K is observed in the temperature dependence of specific heat and magnetic susceptibility. A very large softening beyond 50% from 300 down to 7.0 K is also observed in the temperature dependence of the elastic constant of the C_{11}-C_{12} mode. The results reveal clearly that the anomaly at 7.0 K ($=T_Q$) originates from a ferroquadrupolar ordering with an orthorhombic γ-symmetry-lowering mode. Separation between the ground and the first excited singlet states of $4f$ levels is so small in the quadrupolar ordered phase and a transition probability between these states is so extremely large that there occurs a Van Vleck antiferromagnetic transition at 3.2 K by exchange-induced magnetic moments arising from the transition between the ground and the first excited singlet states. [S0163-1829(98)03634-0]

I. INTRODUCTION

The study of the quadrupolar interaction in rare-earth intermetallic compounds has been developed greatly during the last couple of decades.[1] In particular, quadrupolar orderings have been found in paramagnetic states of cubic TmCd, TmZn, and so on.[2–4] It is considered that the ordering originates cooperatively from the quadrupolar interaction between different $4f$ ions and the magnetoelastic interaction. Furthermore, it is known that the quadrupolar interaction influences magnetic properties severely. First-order magnetic transitions occur accompanied by a lattice distortion as in TbP and DySb.[5–8] Under the influence of quadrupolar interaction, DyCu has a triple-q antiferromagnetic structure where the Dy moments align noncollinearly along threefold axes in the cubic symmetry.[9] It becomes increasingly clear that the quadrupolar interaction plays an important role in magnetic transitions or magnetic structures.

Magnetic behaviors in a rare-earth compound are described by (1) the crystalline electric field (CEF) acting on the $4f$ ion, (2) the interaction between the $4f$ magnetic moment and applied magnetic fields (Zeeman coupling), (3) the exchange interaction between the $4f$ magnetic moments, (4) the magnetoelastic interaction between the $4f$ ion and the lattice, and (5) the quadrupolar interaction between the $4f$ quadrupolar moments. Magnetic ordering occurs by the exchange interaction between the $4f$ magnetic moments and lattice distortion sometimes occurs due to magnetostriction through the magnetoelastic coupling. In other structural phase transitions, there is the well-known cooperative Jahn-Teller distortion caused by the magnetoelastic interaction. According to the Jahn-Teller theorem, the magnetoelastic modulation of the CEF corresponds to an energy gain by degenerate $4f$ orbitals which is larger than the elastic energy loss at the thermodynamic equilibrium. These properties have been extensively studied in many systems with an orbital degeneracy as reported for cubic spinels, in particular, in mixed chromites.[10] Such a phenomenon occurs in the rare-earth insulator $TmVO_4$ with a tetragonal zircon structure.[11] The interaction in the cooperative Jahn-Teller effect is mediated by phonons in these insulators.

On the other hand, in rare-earth intermetallics, the quadrupolar interaction, which is mediated by conduction electrons, dominates the magnetoelastic coupling. Depending on the sign of the quadrupolar interaction, ferroquadrupolar or antiferroquadrupolar ordering occurs. For example, the ferroquadrupolar orderings are realized in TmCd and TmZn,[2–4] and the antiferroquadrupolar orderings are realized in CeB_6 and $PrPb_3$.[12,13] Generally, the quadrupolar interaction is weaker than the magnetic interaction, so there are not many compounds showing quadrupolar ordering. In other words, the quadrupolar orderings were almost observed in Tm, Ce, and Pr intermetallic compounds where the rare-earth ions have weak magnetic interactions compared to other rare earths. For studying the magnetoelastic and quadrupolar interactions, the measurement of elastic constants using ultrasonic pulse is important. The elastic constants reflect the coupling of the strain caused by ultrasonic stress to the quadrupolar moment, which is described by the orbital character of the

CEF state. Therefore, it is also necessary to know the CEF exactly.

As mentioned above, quadrupolar interactions have been studied mainly for compounds with cubic symmetry, since high symmetry is advantageous for the degeneration of $4f$ levels. However, the quadrupolar ordering occurs possibly in lower symmetries such as tetragonal or hexagonal types. Very recently, Morin and Rouchy found the quadrupolar ordering in a tetragonal $TmAg_2$ compound with a $MoSi_2$-type structure.[14] The ferroquadrupolar ordering occurs at 5 K, and the structure transforms simultaneously with an orthorhombic γ-symmetry-lowering mode.

In the present work, we study the magnetic and mag--netoelastic properties of $TmAu_2$ which is isostructural to $TmAg_2$ with the space group $I4/mmm$. $TmAu_2$ undergoes a transition to an antiferromagnetic state at T_N of 3.2 K and the antiferromagnetic structure is the sinusoidally moment-modulated one described by a propagation vector of $\boldsymbol{q}=(\delta\ \delta\ 0)$ with $\delta=0.392$.[15] Our interest is focused on the roles of quadrupolar interaction between Tm^{3+} ions in this magnetic system. We performed magnetic susceptibility, magnetization process, specific heat, ultrasonic velocity, and inelastic neutron spectroscopy (INS) measurements. The CEF levels and eigenfunctions are determined by the INS and the magnetic susceptibility measurements. The ultrasonic velocity associated with different symmetry-lowering modes of the tetragonal cell leads us to conclude that ferroquadrupolar ordering with orthorhombic symmetry occurs at $T_Q=7.0$ K in $TmAu_2$. The results are discussed in the basis of the CEF levels. We also calculated the CEF levels in the quadrupolar ordered state taking the quadrupolar interaction into account which is deduced from ultrasonic velocity measurements. As a result, the antiferromagnetic ordering at $T_N=3.2$ K in $TmAu_2$ which has the singlet ground state is realized due to a large transition probability between the ground and the first excited states around T_N. Therefore, we conclude that there occurs an exchange-induced Van Vleck antiferromagnetic transition at T_N.

II. EXPERIMENTAL

A sample compound was synthesized by a conventional argon arc technique. To ensure homogeneity, the ingot was turned over and remelted several times. A powdered sample was obtained from the ingot annealed at 900 °C for a week in tantalum foil, which was sealed in an evacuated quartz tube. The x-ray powder diffraction pattern measured using Cu-K_α radiation exhibits only the lines characteristic of the $MoSi_2$-type structure, which was interpreted well by the lattice parameters of $a=3.645$ Å and $c=8.890$ Å whose values are in good agreement with those reported previously within experimental error.[15] It was also confirmed that the sample was a single-phase compound since no indication of a secondary phase was found after annealing. The single crystal was grown by the Czochralski method using a triarc furnace. The single-crystalline samples were shaped into a sphere with diameter of about 3 mm for the magnetization measurements and into a rectangle with about $3\times3\times3$ mm^3 for the ultrasonic velocity measurement.

The temperature dependence of the magnetic susceptibility was measured in the range 2.8–300 K using a superconducting quantum interference device (SQUID) magnetometer. Magnetization process was measured using a vibrating-sample magnetometer under magnetic fields up to 150 kOe. The high magnetic fields were produced using a water-cooled Bitter-type magnet at the High Field Laboratory for Superconducting Materials (HFLSM) in Tohoku University. The specific heats under magnetic fields were measured between 1.5 and 100 K using a usual adiabatic method. The elastic constants were determined from the velocity measurements of ultrasonic transverse wave propagating along the *a*, *c*, and 110 axes by a phase-comparison method. The inelastic neutron spectroscopy experiments in order to determine the CEF parameters were performed by a crystal-analyzer-type spectrometer (CAT) at the spallation neutron source (KENS) in the National Laboratory for High Energy Physics in Japan. The energy of the scattered neutrons of the CAT is fixed at 3.9 meV by a pyrolytic graphite crystal analyzer, where the energy resolution is $\Delta\varepsilon/\varepsilon\sim2\%$ in a wide energy range of 1–1000 meV.[16]

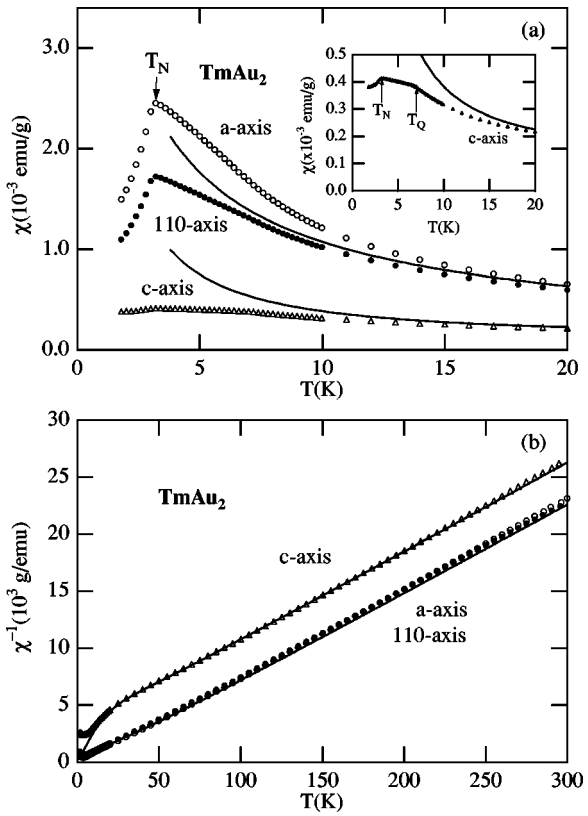

FIG. 1. (a) Temperature dependence of the magnetic susceptibilities of single-crystalline $TmAu_2$ along the *a* (circles), *c* (full circles), and 110 axes (triangles) where the magnetic field of 1 kOe is applied. The inset shows the susceptibility along the *c* axis in a precise scale. (b) Temperature dependence of the reciprocal susceptibilities along the *a* (open circles), *c* (full circles), and 110 axes (triangles) of $TmAu_2$. The solid lines indicate calculated susceptibilities along the *a* and *c* axes using the CEF parameters (see text).

III. RESULTS AND DISCUSSION

Figure 1(a) shows the temperature dependence of the magnetic susceptibilities χ, along the *a*, *c*, and 110 axes of the single-crystalline $TmAu_2$. These were measured under an

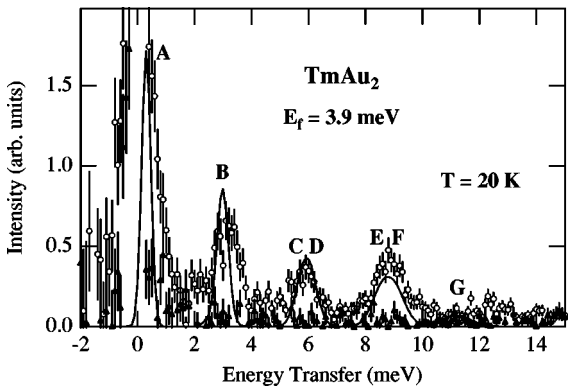

FIG. 2. Inelastic neutron spectra of $TmAu_2$ (open circles) and YAu_2 (triangles) at 20 K. The solid line is fitting curve using the CEF parameters (see text). The peaks A, B, D, E, and F indicate the transitions from the ground state $\Gamma_5^{(1)}$ to $\Gamma_1^{(1)}$, $\Gamma_3^{(2)}$, $\Gamma_5^{(2)}$, Γ_2, and $\Gamma_4^{(1)}$, respectively (see Table I). The peaks C and G show the transitions from the first excited state $\Gamma_1^{(1)}$ to $\Gamma_5^{(2)}$ and $\Gamma_5^{(3)}$, respectively.

applied field of 1 kOe in order to avoid a field-induced transition which occurs at a low magnetic field as described later. The Néel temperature is determined to be $T_N=3.2$ K from antiferromagnetic cusps observed clearly in the χ-T curves along the a and 110 axes. The magnetic susceptibilities at low temperatures, unexpectedly, are not isotropic in the basal plane in spite of the tetragonal symmetry. The inset in the figure shows again the temperature dependence of the magnetic susceptibility along the c axis in a precise scale. A small anomaly is surely observed at 7.0 K in addition to the anomaly at T_N. It is noted that the anomaly at 7.0 K is rather smaller than an expected value originating from a magnetic ordering. This anomaly at 7.0 K is similar to that originating from the quadrupolar ordering in $TmAg_2$.[14] It will be clarified that the anomaly at 7.0 K originates from a ferroquadrupolar ordering, which will be evidenced by the other experimental results and discussed on the basis of the $4f$ levels under the CEF calculation. As shown in Fig. 1(b), the reciprocal susceptibility χ^{-1}-T curves along the a, c, and 110 axes satisfy the Curie-Weiss law above 50 K. Paramagnetic Curie temperatures are determined to be $\theta_p^a=10.23$ K, $\theta_p^{110}=1.90$ K, and $\theta_p^c=-29.74$ K, respectively. Effective paramagnetic moments are also determined to be $\mu_{\rm eff}^a=7.51\mu_B$/f.u., $\mu_{\rm eff}^{110}=7.67\mu_B$/f.u., and $\mu_{\rm eff}^c=7.47\mu_B$/f.u., respectively, whose values almost agree with the theoretical one of $7.56\mu_B$ for the Tm^{3+} ion. In Figs. 1(a) and 1(b), the solid lines are calculated using the CEF parameters determined by the results of the INS, magnetic susceptibility, and ultrasonic velocity measurements. The calculated curves agree qualitatively with the observed curves.

Figure 2 shows the inelastic neutron scattering spectra of $TmAu_2$ and YAu_2 observed at a scattering angle of 43° at 20 K. The well-defined excitations are observed obviously around 3.0, 5.8, 8.8, and 12.2 meV. All peaks are attributable to those by magnetic excitations, since no peak is found in this energy region in YAu_2 whose spectrum shows a phonon contribution. In the figure, the solid line is a fitted curve using a refined set of the CEF parameters. The broad peaks by phonon scattering are observed at a 16–40 meV region in both spectra of $TmAu_2$ and YAu_2. The temperature dependence of the magnetic susceptibilities, and the inelastic neutron spectra of $TmAu_2$ are explained satisfactorily by a unique set of the CEF parameters obtained by the present procedure. The Hamiltonian for the crystalline electric field interaction $\mathcal{H}_{\rm CEF}$ of the tetragonal symmetry D_{4h} of Tm^{3+} ion is given by

$$\mathcal{H}_{\rm CEF}=B_2^0O_2^0+B_4^0O_4^0+B_4^4O_4^4+B_6^0O_6^0+B_6^4O_6^4. \qquad (1)$$

Here, O_l^m is the Stevens equivalent operators expressed by the angular momentum J_x, J_y, and J_z. The $4f$ multiplet of Tm^{3+} $(J=6)$ split into seven singlets and three doublets $(2\Gamma_1+\Gamma_2+2\Gamma_3+2\Gamma_4+3\Gamma_5)$. The eigenfunctions and allowed transitions among these CEF levels have been summarized by Blanco, Gignoux, and Schmitt.[20] The B_2^0 value is at first estimated approximately from the reciprocal susceptibilities of the single crystal using the relations as follows:[17]

$$\chi_{[001]}^{-1}-\chi_{[110]}^{-1}=\frac{3}{2}\,\frac{(2J-1)(2J+3)}{5C}B_2^0,$$

$$\chi_{[001]}^{-1}(T)+2\chi_{[110]}^{-1}(T)=3\frac{T-\theta^*}{C}, \qquad (2)$$

where C is the Curie constant and θ^* the paramagnetic Curie temperature. From the present data as shown in Fig. 1(b), $\Delta\chi^{-1}(=\chi_{[001]}^{-1}-\chi_{[110]}^{-1})$ is estimated to be 37.27 kOe/μ_B at 300 K. The average of the Curie constant is determined to be 1.285 kOe/μ_B ($7.57\mu_B$/f.u.). From Eq. (2), consequently, the B_2^0 and θ^* values are estimated to be 0.970 and -7.03 K, respectively. This B_2^0 value was used as the initial parameter in order to estimate the four B_4^m and B_6^m parameters. These parameters should explain the CEF level obtained from the INS spectra and the susceptibility curves. The fitting was done based on the expressions of magnetic susceptibility.[19] The CEF parameters are refined to be $B_2^0=0.967$ K, $B_4^0=0.950$ mK, $B_4^4=-5.27$ mK, $B_6^0=0.163$ mK, and $B_6^4=1.20$ mK. Table I summarizes the CEF level spacing and eigenfunctions. The analysis reveals that the ground state is a $\Gamma_5^{(1)}$ doublet and the first excited state $\Gamma_1^{(2)}$ is a singlet which locates at 3.58 K from the ground state.

The temperature dependence of the elastic constants, transverse C_{66}, C_{44}, and C_{11}-C_{12} ultrasonic modes, are shown in Fig. 3. A very large softening beyond 50% from 300 down to 7.0 K was observed in the C_{11}-C_{12} mode. This fact is surely one of the results which evidences the occurrence of the quadrupolar ordering at $T_Q=7.0$ K. Such a phenomenon is very similar to that of $TmAg_2$.[14] The dotted line indicates C_0^γ which is the elastic constant if the quadrupole-strain interaction is switched off in the figure. The solid line is a fitted curve using the CEF, magnetoelastic, and quadrupolar interaction parameters. The elastic energy of the crystal can be expressed by the elastic strain. The ultrasonic pulse induces the elastic strain, which perturbs the CEF levels of $4f$ electrons. The microscopic origin of this interaction can be considered as the quadrupolar moment of the $4f$ electronic states with an orbital angular moment coupled to the appropriate strains. The interaction between the quadrupolar moment and the elastic strain appears sensitively in the temperature dependence of elastic constants.

TABLE I. All eigenfunctions calculated using the CEF parameters of $B_2^0=0.967$ K, $B_4^0=0.950$ mK, $B_4^4=-5.27$ mK, $B_6^0=0.163$ mK, and $B_6^4=1.20$ mK.

Energy (K)	Label Γ_i	Eigenfunctions
209.0	$\Gamma_4^{(2)}$	$-0.6224\|-6\rangle-0.3356\|-2\rangle+0.3356\|2\rangle+0.6224\|6\rangle$
198.1	$\Gamma_3^{(1)}$	$-0.6796\|-6\rangle-0.1954\|-2\rangle-0.1954\|2\rangle-0.6796\|6\rangle$
133.3	$\Gamma_5^{(3)}$	$-0.9467\|-3\rangle+0.2983\|1\rangle+0.1215\|5\rangle$
		$0.1215\|-5\rangle+0.2983\|-1\rangle-0.9467\|3\rangle$
105.0	$\Gamma_4^{(1)}$	$0.3356\|-6\rangle-0.6224\|-2\rangle+0.6224\|2\rangle-0.3356\|6\rangle$
99.4	$\Gamma_1^{(2)}$	$0.7065\|-4\rangle+0.0431\|0\rangle+0.7065\|4\rangle$
99.2	Γ_2	$-0.7071\|-4\rangle-0.7071\|4\rangle$
70.6	$\Gamma_5^{(2)}$	$0.2657\|-3\rangle+0.5098\|1\rangle+0.8182\|5\rangle$
		$0.8182\|-5\rangle+0.5098\|-1\rangle+0.2657\|3\rangle$
34.6	$\Gamma_3^{(2)}$	$-0.1954\|-6\rangle+0.6796\|-2\rangle+0.6796\|2\rangle-0.1954\|6\rangle$
3.6	$\Gamma_1^{(1)}$	$-0.0305\|-4\rangle+0.9991\|0\rangle-0.0305\|4\rangle$
0.0	$\Gamma_5^{(1)}$	$-0.1821\|-3\rangle-0.8069\|1\rangle+0.5619\|5\rangle$
		$0.5619\|-5\rangle-0.8069\|-1\rangle-0.1821\|3\rangle$

Theoretical description of the interaction has been studied by many researchers.[10,18,21] In many intermetallic rare-earth compounds, the quadrupolar interaction also influences the temperature dependence of the elastic constants.[22] The scattering of the conduction electrons by the electric quadrupolar moments of $4f$ electrons leads to a quadrupolar interaction such as the RKKY mechanism. When the quadrupolar moment at different rare-earth ion sites fluctuates incoherently, the molecular field approximation (MFA) is applicable. Both the quadrupolar and magnetoelastic terms can be grouped together in the total quadrupolar Hamiltonian[14]

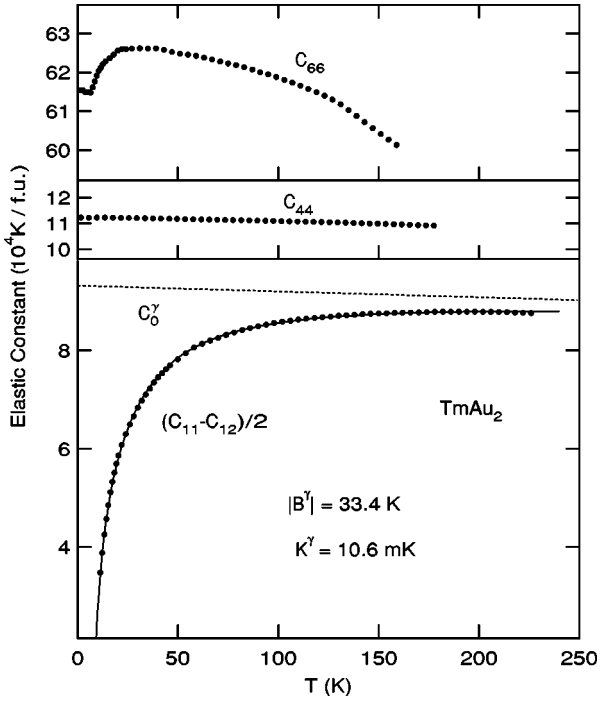

FIG. 3. Temperature dependence of the elastic constants of transverse C_{66}, C_{44}, and C_{11}-C_{12} modes. The C_0^γ is the back ground elastic constant deduced from the CEF calculation. The solid line is the calculated curve.

$$\mathcal{H}_{\mathrm{QT}}=-G^\alpha\langle O_2^0\rangle O_2^0-G^\gamma\langle O_2^2\rangle O_2^2-G^\delta\langle P_{xy}\rangle P_{xy}-G^\varepsilon[\langle P_{yz}\rangle P_{yz}+\langle P_{zx}\rangle P_{zx}], \tag{3}$$

where the total quadrupolar parameters G^μ are defined as

$$G^\alpha=\frac{(B^{\alpha1})^2C_0^{\alpha2}-2B^{\alpha1}B^{\alpha2}C_0^{\alpha12}+(B^{\alpha2})^2C_0^{\alpha1}}{C_0^{\alpha1}C_0^{\alpha2}-(C_0^{\alpha12})^2}+K^\alpha, \tag{4}$$

$$G^\gamma=\frac{(B^\gamma)^2}{C_0^\gamma}+K^\gamma, \tag{5}$$

$$G^\delta=\frac{(B^\delta)^2}{C_0^\delta}+K^\delta, \tag{6}$$

$$G^\varepsilon=\frac{(B^\varepsilon)^2}{C_0^\varepsilon}+K^\varepsilon. \tag{7}$$

The equivalent operators of quadrupolar moment are expressed as follows: $O_2^0=3J_z^2-J(J+1)$, $O_2^2=J_x^2-J_y^2$, and $P_{ij}=\frac{1}{2}(J_iJ_j+J_jJ_i)$, where $(i,j=xy,yz,zx)$. The B^μ's and K^μ's are the magnetoelastic coefficients and the quadrupolar interaction parameter between the rare-earth ions, respectively. The C^μ's are the elastic constants: $C^{\alpha1}=\frac{1}{3}(2C_{11}+2C_{12}+4C_{13}+C_{33})$, $C^{\alpha2}=-\frac{1}{3}(C_{11}+C_{12}-4C_{13}+2C_{33})$, $C^\gamma=C_{11}-C_{12}$, $C^\delta=2C_{66}$, and $C^\varepsilon=2C_{44}$. The experimental results of the temperature dependence of the elastic constants reveal that an orthorhombic γ-symmetry lowering mode is dominant, and hence the following discussion will be limited to the γ mode. The temperature dependence of elastic constants is described by treating the quadrupole-strain interaction as a perturbation:[18]

$$C^\gamma(T)=C_0^\gamma(T)-(B^\gamma)^2\frac{\chi_\gamma(T)}{1-K^\gamma\chi_\gamma(T)}, \tag{8}$$

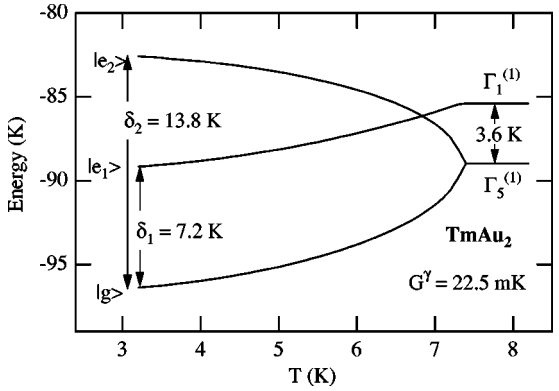

FIG. 4. Temperature dependence of the low-lying CEF levels calculated between T_Q and T_N.

where $C_0^{\gamma}(T)$ is the background when there exists no magnetic interaction. $\chi_{\gamma}(T)$ is the well-known strain susceptibility which implies the quadrupolar response of the $4f$-electronic system.[23]

The analysis for the elastic softening in C_{11}-C_{12} mode provides $B^{\gamma}=33.4$ K and $K^{\gamma}=10.6$ mK. The total quadrupolar parameter is given $G^{\gamma}=22.5$ mK. This quadrupolar ordering is ferrotype because of $K^{\gamma}>0$.

In the quadrupolar ordered phase between T_Q and T_N, the crystal structure is considered to transform from tetragonal to orthorhombic which is caused by the ferroquadrupolar ordering. The strain originated from quadrupolar ordering is an orthorhombic γ-symmetry-lowering mode, and then the ordering parameter is $\langle O_2^2\rangle$. Taking the dominant γ strain mode into account, the Hamiltonian is rewritten as

$$\mathcal{H}=\mathcal{H}_{\mathrm{CEF}}-G^{\gamma}\langle O_2^2\rangle O_2^2. \tag{9}$$

The ordering parameter $\langle O_2^2\rangle$ depending on temperature can be obtained by self-consistent diagonalization of Eq. (9) and minimization of the free energy $F(T)=-T\ln Z+(G^{\gamma}/2)\langle O_2^2\rangle^2$ with regard to $\langle O_2^2\rangle$. The calculated result of the temperature dependence of low-lying CEF levels between T_Q and T_N is shown in Fig. 4. The present CEF model predicts that the ground state $\Gamma_5^{(1)}$ doublet separates below T_Q accompanying with the structural phase transition caused by the ferroquadrupolar ordering, that is, the one singlet ($|g\rangle$) goes toward the lowest energy, and the other singlet ($|e_2\rangle$) goes toward higher energy with decreasing temperature below T_Q. The separation between $|g\rangle$ and $|e_2\rangle$ is $\delta_2=13.8$ K at T_N. On the other hand, the first excited $\Gamma_1^{(2)}$ singlet lowers and approaches the new singlet ground state $|g\rangle$ with decreasing temperature and locates in a lower energy level than the $|e_2\rangle$ singlet just below T_Q. The separation between $|g\rangle$ and $|e_1\rangle$ is $\delta_1=7.2$ K at T_N.

Figure 5(a) shows the temperature dependence of the specific heat of $TmAu_2$ under magnetic fields of 0 and 5.5 kOe along the a axis, where the specific heat of the isostructural YAu_2 compound is also shown by solid lines. The phonon contribution estimated from the specific heat of YAu_2 is negligibly small below 10 K compared with the magnetic part in $TmAu_2$. Under zero magnetic field, anomalous specific heats are observed at 3.2 and 7.0 K, which originate from the antiferromagnetic ordering and the ferroquadrupolar ordering, respectively. Under the field of 5.5 kOe, the anomalous specific heats are observed at 2.2, 2.5, and 7.0 K. The newly appeared transition at 2.2 K corresponds well to the field-induced transition from the antiferromagnetic state to an intermediate one at H_{c1}^{a} shown in Fig. 6(a) as described later. Figure 5(b) shows the temperature dependence of the entropy of the electronic contribution under zero field. It is remarkable that the value of the entropy reaches nearly $R\ln 2$ around T_N and reaches nearly $R\ln 3$ around T_Q. This result is explained well by the present CEF model, that is, the ground state $\Gamma_5^{(1)}$ doublet and the first excited $\Gamma_1^{(2)}$ singlet are regarded as a pseudotriplet above T_Q. The ground state $|g\rangle$ singlet and the first excited $|e_1\rangle$ singlet behave as a pseudo-doublet between T_Q and T_N. We note that the antiferromagnetic transition occurs at $T_N=3.2$ K in $TmAu_2$ in spite of the singlet ground state $|g\rangle$ in the quadrupolar ordered phase. The transition probability between the ground $|g\rangle$ and the first excited $|e_1\rangle$ singlet states is extremely large compared to several other transitions at temperatures between T_Q and T_N. Therefore, the magnetic transition realized in $TmAu_2$ is a Van Vleck antiferromagnetic one occurring because of an exchange induced magnetic moment between the ground $|g\rangle$ and the first excited $|e_1\rangle$ singlets. When two singlets are separated by an energy δ and neglecting all the other states, determination of the pole of $\chi(\mathbf{q},\omega,T)$ gives the following relation according to the random phase approximation (RPA)[19]

$$\omega(\mathbf{q})=\delta\left\{1-\frac{2}{\delta}|M|^2J(\mathbf{q})\tanh\left(\frac{\delta}{2T}\right)\right\}^{1/2}, \tag{10}$$

where $J(\mathbf{q})$ is the Fourier transformation of bilinear magnetic exchange integral and M the transition probability be-

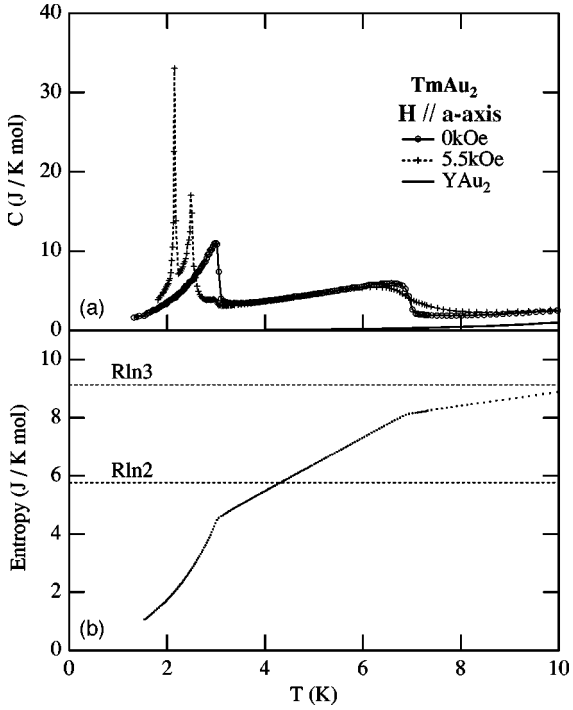

FIG. 5. (a) Temperature dependence of the specific heat of $TmAu_2$ under the applied magnetic field of 0 (open circles) and 5.5 kOe (crosses). The solid line shows that of YAu_2. (b) Temperature dependence of the entropy in $TmAu_2$ without the applied field.

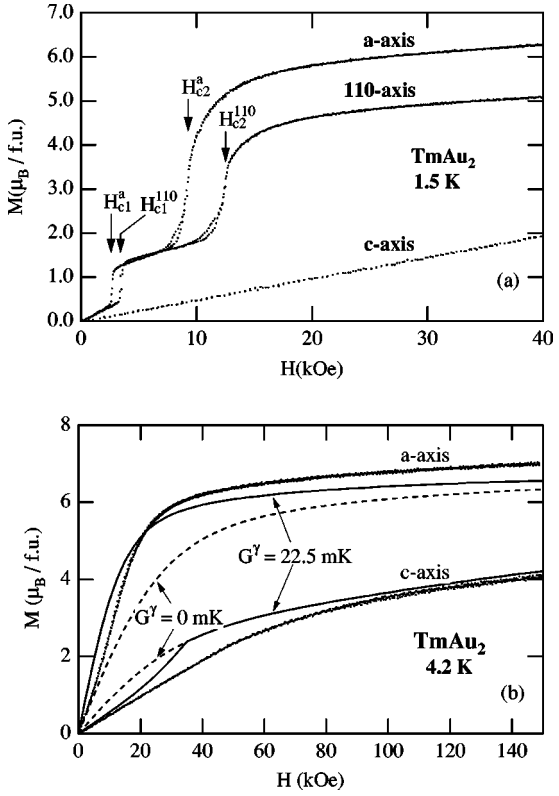

FIG. 6. (a) Magnetization curves of $TmAu_2$ at 1.5 K in magnetic fields up to 50 kOe along the *a*, 110, and *c* axes. (b) The observed and the calculated magnetization processes along the *a* and *c* axes at 4.2 K in the quadrupolar ordered state. The dots indicate the observed curve. The solid and the broken lines indicate the calculated curves using G^{γ} of 22.5 and that of 0 mK, respectively.

tween the two levels. As is clear in this equation, when the $|M|^2J(\mathbf{q})$ value is so large that the $\omega(\mathbf{q})$ value becomes zero, a magnetic transition occurs in spite of the singlet ground state. In the case of $TmAu_2$, it is obtained to be $|M|^2 = 40.46$ and $J(\mathbf{q}) = 0.11$ K in the condition of $\omega(\mathbf{q}) = 0$ at $T_N = 3.2$ K and $\delta = 7.2$ K. Usually, the value of $J(\mathbf{q})$ in Tm compounds with a doublet ground state is estimated to be about T_N. In $TmAu_2$, $J(\mathbf{q})$ is much smaller than in the usual cases. In $TmAg_2$ with the same crystal structure as $TmAu_2$, no magnetic transition occurs.[14] The low-lying CEF levels in $TmAg_2$ consist of the ground state $\Gamma_5^{(1)}$ doublet and the first excited state $\Gamma_1^{(2)}$ singlet which have an energy separation of 14.0 K. Even below $T_Q = 5.0$ K, the first excited state remains at a higher level than two singlets separated from the doublet by the quadrupolar ordering. Moreover, the transition probability between the ground and the first excited singlets in the quadrupolar ordered phase is very small compared to that of $TmAu_2$. Consequently, it is considered that a Van Vleck transition in $TmAg_2$ does not even occur.

Figure 6(a) shows the magnetization processes (*M*-*H* curves) at 1.5 K measured in magnetic fields up to 50 kOe along the *a*, 110, and *c* axes, respectively. Two field-induced transitions are observed at $H_{c1}^{a} = 2.7$ kOe and $H_{c2}^{a} = 9.3$ kOe along the *a* axis. A saturation magnetization of $M_{\rm sat}^{a} = 6.9\mu_B$/f.u. is obtained by the *M*-*H* curves measured under the fields up to 150 kOe along the *a* axis. Two field-induced transitions are also observed at $H_{c1}^{110} = 3.4$ kOe and

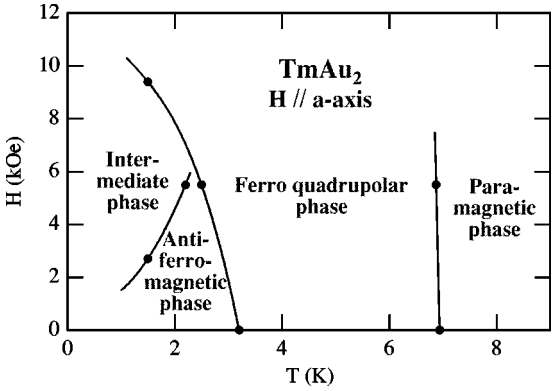

FIG. 7. Phase diagram of $TmAu_2$ under the magnetic fields applied along the *a* axis.

$H_{c2}^{110} = 12.5$ kOe along the 110 axis. High-field measurement also shows that the magnetization reaches a saturation value of $M_{\rm sat}^{110} = 5.2\mu_B$/f.u. The $M_{\rm sat}^{110}$ value is close to the magnetic moment component of $M_{\rm sat}^{a}$ ($4.9\mu_B$/f.u.$= M_{\rm sat}^{a}\cos 45°$). Moreover, H_{c1}^{110} and H_{c2}^{110} are almost $H_{c1}^{a}/\cos 45°$ and $H_{c2}^{a}/\cos 45°$, respectively. These results indicate that the Tm moments align along the *a* axis. It is interesting that the magnetic moments align along the *a* axis with large magnetic anisotropy, although it is expected that the anisotropy is small in the basal plane with tetragonal symmetry. This result ensures that the structural phase transition from tetragonal to orthorhombic phase at T_Q occurs. Figure 6(b) shows the observed and calculated magnetization processes along the *a* and *c* axes in the quadrupolar ordered phase at 4.2 K. The magnetization process between T_Q and T_N can be calculated by diagonalizing the Hamiltonian self-consistently as follows:

$$\mathcal{H} = \mathcal{H}_{\rm CEF} - g_J\mu_B\mathbf{H}\cdot\mathbf{J} - G^{\gamma}\langle O_2^2\rangle O_2^2. \tag{11}$$

The second term expresses the Zeeman coupling between the $4f$ magnetic moment $\mathbf{M} = g_J\mu_B\langle\mathbf{J}\rangle$ and the applied field $\mathbf{H}$ which is corrected for demagnetization effects. In the figure, the dots indicate the observed curve. The solid and the broken lines are the calculated curves using G^{γ} of 22.5 and 0 mK, respectively. The calculated magnetization curves using $G^{\gamma} = 22.5$ mK along the *a* and *c* axes are in good agreement with the observed curves, especially the initial part of the curves, compared to the calculated curves using only the CEF term ($G^{\gamma} = 0$ mK). The anomalous magnetization curve along the *c* axis around 40 kOe indicates the structural phase transition from the orthorhombic to tetragonal phase, where the quadrupolar order is destroyed by the magnetic field. The deviation from the observed value is attributable to the magnetic exchange interaction, since the measured temperature of 4.2 K is just above T_N.

Figure 7 shows the *H*-*T* phase diagram of $TmAu_2$ under the fields applied along the *a* axis which is drawn by the results of the specific heat, magnetization curve, and ultrasonic velocity measurements. The Tm moments are forced to align along the *a* axis with a large magnetic anisotropy, where the tetragonal symmetry above T_Q is broken below T_Q. This originates in the large magnetic anisotropy in the basal plane through the structural transformation.

IV. CONCLUSIONS

In this paper, the study of the magnetic and magnetoelastic properties makes it clear that quadrupolar ordering in tetragonal $TmAu_2$ intermetallics occurs. The analysis of the elastic constant of the C_{11}-C_{12} mode reveals that this quadrupolar ordering is ferroquadrupolar type with an orthorhombic γ-symmetry-lowering mode. The five CEF parameters are deduced from inelastic neutron scattering spectra and the magnetic susceptibilities in $TmAu_2$. Antiferromagnetic ordering also occurs below T_Q. The temperature dependence of the low-lying CEF level scheme between T_Q and T_N was calculated. We conclude that the magnetic transition in $TmAu_2$ is a Van Vleck antiferromagnetic one occurring because of the exchange-induced magnetic moment between the ground and first excited singlets.

A neutron diffraction experiment at low temperatures is now in progress in order to observe the structural phase transition at T_Q and to determine the magnetic structure. It is expected that the quadrupolar interaction severely influences the magnetic structure. Furthermore, we plan to observe the low-lying CEF levels around transition temperatures with high resolution inelastic neutron spectroscopy.

ACKNOWLEDGMENTS

The authors would like to thank Professor K. Suzuki and his collaborators, IMR, for kind support in the magnetometric measurement using the SQUID magnetometer. We would also like to thank Professor T. Suzuki, Department of Physics, Tohoku University, for support in the specific heat measurement. Thanks are also due to the staff of HFLSM, IMR, for operating the high-field magnet.

*Present address: Department of Physics, Saitama University, Urawa 338-8570, Japan.

†Present address: Facility of Engineering, Yamagata University, Jonan 4-3-16, Yonezawa 992, Japan.

‡Present address: Center for Low Temperature Science, Tohoku University, Katahira 2-1-1, Sendai 980-77, Japan.

§Present address: Graduate School of Science and Technology, Niigata University, Igarashi Ninomachi 8050, Niigata 950-21, Japan.

[1] P. Morin and D. Schmitt, in *Ferromagnetic Materials*, edited by K. H. J. Buschow and E. P. Wohlfarth (North-Holland, Amsterdam, 1990), Vol. 5, p. 1.

[2] R. Aléonard and P. Morin, Phys. Rev. B **19**, 3868 (1979).

[3] P. Morin, J. Rouchy, and D. Schmitt, Phys. Rev. B **17**, 3684 (1978).

[4] D. Givord, P. Morin, and D. Schmitt, J. Magn. Magn. Mater. **40**, 121 (1983).

[5] E. Bucher, J. P. Maita, G. W. Hull, Jr., L. D. Longinotti, B. Lüthi, and P. S. Wang, Z. Phys. B **25**, 41 (1976).

[6] J. Kötzler, G. Raffius, A. Loidl, and C. M. E. Zeyen, Z. Phys. B **35**, 125 (1979).

[7] F. Lévy, Phys. Kondens. Mater. **10**, 85 (1969).

[8] E. Bucher, R. J. Birgeneau, J. P. Maita, J. P. Felcher, and T. O. Brun, Phys. Rev. Lett. **28**, 746 (1972).

[9] R. Aléonard, P. Morin, and J. Rouchy, J. Magn. Magn. Mater. **46**, 233 (1984).

[10] M. Kataoka and J. Kanamori, J. Phys. Soc. Jpn. **32**, 113 (1972).

[11] G. A. Gehring and K. A. Gehring, Rep. Prog. Phys. **38**, 1 (1975).

[12] J. M. Effantin, J. Rossat-Mignod, P. Burlet, H. Bartholin, S. Kunii, and T. Kasuya, J. Magn. Magn. Mater. **47&48**, 145 (1985).

[13] P. Morin, D. Schmitt, and E. du Trémolet de Lacheisserie, J. Magn. Magn. Mater. **30**, 257 (1982).

[14] P. Morin and J. Rouchy, Phys. Rev. B **48**, 256 (1993).

[15] M. Atoji, J. Chem. Phys. **52**, 6433 (1970).

[16] S. Ikeda and N. Watanabe, Physica B **120**, 131 (1983).

[17] P. Boutron, Phys. Rev. B **7**, 3226 (1973).

[18] P. Levy, J. Phys. C **6**, 3545 (1973).

[19] P. Fulde, in *Handbook on the Physics and Chemistry of Rare Earths*, edited by K. A. Gschneider, Jr. and L. Eyring (North-Holland, Amsterdam, 1979), Vol. 2, p. 295.

[20] J. A. Blanco, D. Gignoux, and D. Schmitt, Z. Phys. B **89**, 343 (1992).

[21] V. Dohm and P. Fulde, Z. Phys. B **21**, 369 (1975).

[22] P. Thalmeier and P. Fulde, Z. Phys. B **22**, 359 (1975).

[23] P. Thalmeier and B. Lüthi, in *Handbook on the Physics and Chemistry of Rare Earths*, edited by K. A. Gschneider, Jr. and L. Eyring (Elsevier Science Publishers, British Vancouver, 1991), Vol. 14, p. 225.